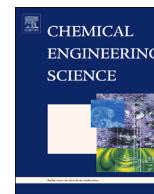




ELSEVIER

Contents lists available at ScienceDirect

Chemical Engineering Science

journal homepage: www.elsevier.com/locate/ces

Geometric effects on lateral transport induced by slanted grooves in a microchannel at a low Reynolds number

Sungchan Yun^a, Geunbae Lim^{a,b,*}, Kwan Hyoung Kang^a, Yong Kweon Suh^{c,**}

^a Department of Mechanical Engineering, Pohang University of Science and Technology (POSTECH), San 31, Hyoja-dong, Pohang 790-784, Republic of Korea

^b Division of Integrative Bioscience and Biotechnology, Pohang University of Science and Technology (POSTECH), San 31, Hyoja-dong, Pohang 790-784, Republic of Korea

^c Department of Mechanical Engineering, Dong-A University, 840 Hadan-dong, Saha-gu, Busan 604-714, Republic of Korea

H I G H L I G H T S

- Lateral transport by a slanted groove is quantified by lateral displacement.
- The cross-movement is numerically investigated for varying groove features.
- The region of cross-movement is identified in the cross section of the channel.
- At high groove angle, lateral transport is characterized by swirls within grooves.
- The swirls within grooves are investigated for varying groove features.

A R T I C L E I N F O

Article history:

Received 10 April 2013

Received in revised form

16 July 2013

Accepted 28 August 2013

Available online 7 September 2013

Keywords:

Slanted groove

Convective transport

Mixing

Numerical analysis

Visualization

Swirling structure

A B S T R A C T

Flow over slanted grooves can generate a high degree of lateral transport by means of cross-movement of fluids along the groove. However, the quantitative relationship between the groove features and the cross-movement of fluid is rarely reported. We investigate the geometric effects of the groove on the cross-movement by computing the lateral displacements of particles in the cross section of the channel for varying geometric parameters of the groove, such as the depth, width, and angle. We identify the region of the cross-movement in the cross section of the channel, discuss the mechanism of material folding by the grooves, and touch on the validity of the effective slip model. The experimental results show the effect of the groove depth on the lateral transport of dye solutions, which confirms the numerical results. At high groove angles, the lateral transport can be characterized by complex swirling structures, and the swirls are quantified by the characteristic number of revolutions inside the groove.

© 2013 Elsevier Ltd. All rights reserved.

1. Introduction

Slanted grooves are a useful design concept for lab-on-a-chip applications such as mixing (Stroock et al., 2002a; Johnson et al., 2002; Kim et al., 2004; Wang et al., 2007; Yang et al., 2008; Tung and Yang, 2008; Tofteberg et al., 2010), separating or sorting (Choi et al., 2007; Hsu et al., 2008; Nishimura et al., 2009), focusing (Xuan et al., 2010), and pumping (Gitlin et al., 2003; Jahanshahi et al., 2012), because of the ability of slanted grooves to effectively induce lateral flow components without external energy sources. The well-known examples of mixers include the staggered

herringbone micromixer (SHM) that creates two count-rotating flows by the asymmetrically arranged herringbone grooves on the bottom surface (Stroock et al., 2002a), and the barrier embedded micromixer that creates two co-rotating flows separated by the alternate barriers on the top of the slanted groove channel (Kim et al., 2004). Such slanted groove patterned mixers could attain rapid convective mixing once a high degree of lateral transport is induced by the cross-movement (CM) of the fluid, which is the nonaxial motion of the fluid along the slanted grooves as observed by Johnson et al. (2002). To quantify the degree of lateral transport by the slanted grooves, the effect of the slanted grooves was analytically represented by the slip velocity boundary condition (Stroock et al., 2002b; Wang, 2003; Stroock and McGraw, 2004; Kirtland et al., 2006; Lopez and Graham, 2008). The slip model provides the slip velocity, which can be derived by the geometric parameters of the groove. However, with a validity that is limited

* Corresponding author. Tel.: +82 54 279 2186.

** Corresponding author. Tel.: +82 51 200 7648.

E-mail addresses: limmems@postech.ac.kr (G. Lim), yksuh@dau.ac.kr (Y.K. Suh).

to shallow grooves, this slip model thus cannot fully explain the CM.

Several studies attempted to analyze CM for varying groove features by using numerical simulations. Hassell and Zimmerman (2006) investigated the effect of groove depth on CM by computing the lateral velocity within the groove. The study reported that limited CM occurs when the grooves are shallow and that an increase in groove depth leads to an increase in the amount of CM, but also to saturation because of the reduced effectiveness of the depth. Lynn and Dandy (2007) also showed the effect of the groove depth and width on the lateral transport by computing the lateral velocity within the groove. Optimizing mixing in slanted groove patterned channels requires the visualization of how the groove features affect CM. Johnson and Locascio (2002) reported that the interface between two fluids gradually becomes more folded as the groove depth increases, which results in rapid mixing. Aubin et al. (2005) showed that the exchange of trace particles between the left and right sides in the cross section of the staggered herringbone micromixer intensifies as the groove depth and width increase. Yang et al. (2005), Ansari and Kim (2007), and Cortes-Quiroz et al. (2009) determined that the ratio of groove depth to channel height strongly affects the mixing pattern. Singh et al. (2008) noted that the critical groove depth at which chaotic advection begins is roughly 20% of the channel height and that mixing patterns and efficiency are not significantly improved for deeper grooves. These results imply that the amount of CM is roughly proportional to the groove depth and width, but the CM associated with groove features cannot be fully understood by using lateral velocity or the mixing patterns of two fluids.

To our knowledge, the effect of groove features on the flow structure within the slanted groove has been rarely investigated, except for that within a two-dimensional (2D) cavity (Taneda, 1979; Shen and Floryan, 1985; Wang, 2003). Based on this study, the vortices inside the cavity considerably change with the ratio of the cavity width to depth (i.e., aspect ratio, AR). When the AR increases to 2.0, a single central vortex begins to evenly divide into two vortices that move apart toward the left and right corners of the cavity at higher ARs (Shen and Floryan, 1985). In the current work, we observed that swirling structures easily developed inside the groove because of an increase in lateral velocity when the inclined angle decreases below 90°. The lateral transport was characterized by the swirling structures at high groove angles. We investigated the swirling structures and the lateral transport depending on the groove width and inclined angle.

Standard microchannels commonly have Reynolds number with low values ($Re = Ul/\nu < 1$) and Péclet number with high values ($Pe = Ul/D > 10^4$), where U , l , ν , and D are the characteristic velocity, characteristic length, kinematic viscosity of fluids, and diffusivity of reagents subject to mixing in the flow, respectively. The parameter values are based on the typical setting: $10^{-4} < U < 10^{-2}$ m/s, $l \sim 10^{-4}$ m, $\nu \sim 10^{-6}$ m²/s, and $D \sim 10^{-12}$ m²/s. The value of D corresponds to a 220 nm radius particle, and D is inversely proportional to the radius based on the well-known Stokes–Einstein relation. In this situation, the mass transfer of the particle by diffusion is very slow compared with that by convection. For example, significant distance along the channel [$l_{diff} \sim U \times (l^2/D) = Pe \times l > 1$ m] is required to allow reagents to diffuse to a reactive boundary, such as in biochemical sensors and fuel cells (Kirtland et al., 2006; Yoon et al., 2006; Lopez and Graham, 2008; Ziegenbalg et al., 2010), based on the aforementioned parameter values. In fast flows ($U > 10^{-2}$ m/s), a longer distance is required because of $l_{diff} \sim U$. Thus, since the convective transport of particles is very important at a low Re and high Pe , this paper handles the Stokes flow at a low Re ($Re < 1$) and high Pe with no account of fluid inertia and species diffusion.

In what follows, we describe the numerical method and experimental setup for flow visualization. We numerically analyze

the CM for the varying geometric parameters of the groove, such as the depth, width, and angle, by computing the lateral displacements using a mapping matrix. In addition, we discuss the region of the CM in the cross section of the channel and the folding mechanism by grooves, and touch on the validity of the slip model. The experiments verify the numerical results on the effect of the groove depth on the lateral transport. Finally, we numerically analyze the swirling structures within the groove.

2. Numerical simulation of fluid flow

We numerically solved the three-dimensional steady state and incompressible Navier–Stokes equations, and continuity equation as

$$\rho \tilde{\mathbf{u}} \cdot \tilde{\nabla} \tilde{\mathbf{u}} + \tilde{\nabla} p - \mu \tilde{\nabla}^2 \tilde{\mathbf{u}} = 0, \quad \tilde{\nabla} \cdot \tilde{\mathbf{u}} = 0 \quad (1)$$

where ρ is the fluid density, $\tilde{\mathbf{u}}$ is the velocity vector, p is the pressure, and μ is the Newtonian viscosity. The computational domain is the rectangular channel including grooves at the bottom of the channel, with channel width of $2\tilde{w} = 200$ μm , channel height of $2\tilde{h} = 80$ μm , groove depth of \tilde{d}_g , groove period of $\tilde{\lambda}$, groove width of $\tilde{\lambda}/2$, and groove angle of θ (Fig. 1). We used the Cartesian coordinates $(\tilde{x}, \tilde{y}, \tilde{z})$ centered at the inlet and the translated coordinates $(\tilde{x}', \tilde{y}', \tilde{z}')$, which are obtained by rotating the \tilde{x} - and \tilde{z} -axis about the \tilde{y} -axis by θ to align \tilde{x}' along the groove. The coordinates are normalized by using three length scales, \tilde{w} , \tilde{h} , and $\tilde{\lambda}$: $x \equiv \tilde{x}'/\tilde{w}$, $y \equiv \tilde{y}'/\tilde{h}$, and $z \equiv \tilde{z}'/\tilde{\lambda}$; $x' \equiv \tilde{x}'/\tilde{w}$, $y' \equiv \tilde{y}'/\tilde{h}$, and $z' \equiv \tilde{z}'/\tilde{\lambda}$. The dimensionless geometric parameters of grooves are $d_g \equiv \tilde{d}_g/2\tilde{h}$ and $\lambda \equiv \tilde{\lambda}/\tilde{\lambda}_{ref}$ ($\tilde{\lambda}_{ref} = 100$ μm). A reference channel was set at $d_g = 0.50$, $\lambda = 1.0$, and $\theta = 45^\circ$, and the various groove features were investigated (Table 1). Water at 25 °C and 1 atm was used as the fluid and Reynolds number ($Re = \rho \langle \tilde{u}_z \rangle \tilde{d}_h / \mu$) was fixed at 0.011 in the numerical study, where $\langle \tilde{u}_z \rangle$ is the spatially averaged axial velocity component at the inlet, and \tilde{d}_h is the hydraulic diameter of the rectangular channel. We used the finite volume CFD package CFX to solve the governing equations. In the low Re regime ($Re < 1$), the flow is considered as the Stokes flow, and the inertia terms in the governing equation may be negligible. However, we employed the full Navier–Stokes equations that require no additional computational load.

The no-slip boundary condition was applied to the solid walls. We imposed the periodic boundary condition on the inlet and outlet for all the variables except for the pressure. We set a pressure difference between the inlet and the outlet to apply a fixed flow rate for all cases. When the velocity field over one periodic unit was computed, the field was used to track particles over numerous periodic domains. The number of grids used in this system amounts to about 1.5 million elements, which is sufficient to ensure that the flow field is independent of the grid resolution. The normalized residuals for the velocity field and the continuity equation are less than 10^{-8} and 10^{-4} , respectively.

A mapping method based on particle tracking (Singh et al., 2008; Kang et al., 2008) was adopted to examine the lateral displacement of the fluid. This method is often used to study the transport of a conservative quantity without considering molecular diffusion (Spencer and Wiley, 1951). The mapping matrix (Φ) contains information on the transport of fluids, i.e., mapping of the fluid particle distribution from the initial to final state in the cross section of interest. The elements of Φ were obtained from the tracking particles in the periodic flow field. Fig. 2 shows that the uniformly distributed particles in an arbitrary cell c_j on a cross sectional plane at $z = z_0$ were tracked along the direction of the main flow, and that the locations of the advected particles were recorded at $z = z_0 + \Delta z$. Element (Φ_{ij}) was defined as the fraction of the flux of c_j donated to c_i , as follows: $\Phi_{ij} = n_{ij}/n_j$, where n_{ij} is the

Download English Version:

<https://daneshyari.com/en/article/6591446>

Download Persian Version:

<https://daneshyari.com/article/6591446>

[Daneshyari.com](https://daneshyari.com)